Quantum-well states in thin Ag films grown on the Ga/Si(111)-$\sqrt{3} \times \sqrt{3}$ surface

S. Starfelt,[*] H. M. Zhang, and L. S. O. Johansson
Department of Engineering and Physics, Karlstad University, SE-651 88 Karlstad, Sweden

(Received 20 October 2017; revised manuscript received 10 April 2018; published 17 May 2018)

Silver thin films have been created by room temperature deposition on a Ga/Si(111)-$\sqrt{3} \times \sqrt{3}$ surface and their valence band structures and core levels have been measured by angle-resolved photoelectron spectroscopy (ARPES). Discrete quantum-well states (QWSs) quantized from the Ag *sp* valence band are observed already at 3 monolayers (ML). The characteristics of the QWSs have been examined in the phase accumulation model for thicknesses between 3 and 12 ML. The phase shift and QWSs binding energies dependence with Ag film thicknesses have all been consistently derived. In-plane energy dispersion follows a parabolic curve, and the effective mass of the QWSs shows an increasing trend with binding energies as well as with reduced film thicknesses. Furthermore, the ARPES measurements reveal umklapp mediated QWSs around the $\overline{M}$ points of the Si(111) 1×1 surface Brillouin zone. The study confirms that the Ga/Si(111)-$\sqrt{3} \times \sqrt{3}$ surface is a good substrate for growing uniform ultrathin Ag films in room temperature conditions.

DOI: 10.1103/PhysRevB.97.195430

I. INTRODUCTION

Low-dimensional systems have long been of interest both for study of fundamental physics and for use in technological applications [1]. One such type of system is metallic thin films, where electrons are spatially confined between the substrate/thin film energy barrier and the vacuum level at the film surface. Electrons that are spatially confined in at least one dimension exhibit energy quantization. In metallic thin films, the discrete energy levels formed follow a nearly free electron (parabolic) dispersion and form what is typically referred to as quantum-well states (QWSs) [1]. QWSs in thin films have been studied thoroughly for many different kinds of substrate/thin film combinations [2–30]. It has been revealed, for example, that measurements of the QWSs can be used to determine the bulk band structure of Ag [13,15]. One common type of combination studied is silver film on a semiconductor substrate, due to its potential use for device applications in the semiconductor industry [2–12]. Two examples are Ag/Ge(111) and Ag/Si(111) thin films [2–11].

The first reported measurement of QWSs in Ag films on Si was made by Wachs *et al.* [2], observing quantum-well peaks for film thicknesses of 5 monolayers (ML) up to 15 ML. Measurements of Ag films on different surface reconstructions of Si(111), such as H-passivated Si(111) [4] or the 7×7 surface [3], highlight the interface importance for the band dispersion and characteristics of the QWSs. Two such substrate dependent characteristics are the phase shift that the electron wave accumulates on reflection at the Ag film boundaries and the in-plane effective mass of the electrons in the QWS bands. A third substrate dependent feature is the effect of the Si dopant type, where highly doped n-type substrates give rise to fine-structure fringes in the QWSs, in contrast to lightly doped n-type or p-type Si samples [6]. The Ag/Ge(111) system has been used to study the phase shift and film thickness effect on the in-plane effective mass [9], as well as revealing the existence of umklapp mediated quantum-well states [7]. In addition, the above mentioned works have contributed to, and successfully applied, the phase accumulation model (PAM), a theoretical framework for understanding the characteristics of QWSs in thin films.

One tedious procedure in the growth of Ag/Si(111) and Ag/Ge(111) systems is that the silver films typically have to be deposited while the substrate is held at low temperatures (LT, around 100 K), followed by annealing to room temperature (RT) in order to achieve sharp QWS features in the photoemission spectra [1,3]. Another issue is the difficulty of observing QWSs for Ag film thicknesses lower than 5 ML [3,4]. An ability to create ultrathin silver films on a silicon substrate at RT conditions would thus be of great scientific challenge. One idea is to modify the substrate/thin film interface by terminating all the Si dangling bonds but still leave enough sticking force. Similar methods have previously been used at LT in order to grow uniform Pb films on metal-terminated Si(111), which allowed for observation of QWSs for coverages as low as 1 ML [24]. Recently, He *et al.* [31] showed that Ag can be grown on Si(111) under RT conditions by introducing a Ga/Si(111)-$\sqrt{3} \times \sqrt{3}$ surface as a buffer layer. The growth mechanism first followed one layer of 1D chains which were suppressed by 2 ML Ag islands, after which it changed to follow a layer-by-layer growth mode. Inspired by these results, this paper studies Ag thin films grown in RT conditions, and explores coverages below 5 ML.

This article presents electronic structure measurements performed on Ag thin films grown on a Ga/Si(111)-$\sqrt{3} \times \sqrt{3}$ surface at RT, with film thicknesses from 3 to 12 ML. The measurements were done with synchrotron based angle-resolved photoelectron spectroscopy (ARPES). ARPES is a great method to probe the electron band structure, as it directly provides the energy dispersion in k space parallel to the surface plane. The band structure reveals distinct quantum-well states

[*]samuel.starfelt@kau.se

2469-9950/2018/97(19)/195430(9) ©2018 American Physical Society

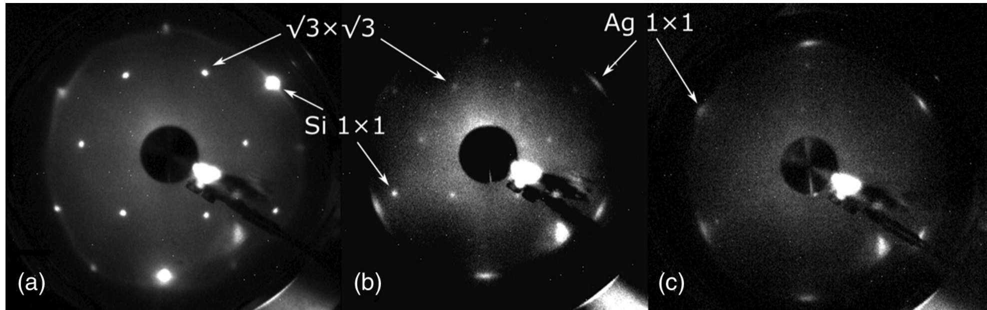

FIG. 1. LEED images of (a) the clean Ga/Si(111)-$\sqrt{3} \times \sqrt{3}$ surface taken at 79.4 eV, (b) 3 ML Ag film on the Ga/Si(111)-$\sqrt{3} \times \sqrt{3}$ surface taken at 131.0 eV, and (c) 9 ML Ag film on the Ga/Si(111)-$\sqrt{3} \times \sqrt{3}$ surface taken at 131.0 eV.

for the measured Ag film thicknesses. Characteristics of the QWSs have been analyzed within the phase accumulation model [17]. The model is found to be in good agreement with the experimental data for Ag films on the Ga/Si(111)-$\sqrt{3} \times \sqrt{3}$ surface. Comparison with other works shows that the phase shift is close to that of the Ag/Si(111)-7 × 7 system [3], but the in-plane effective mass trend follows that of Ag/Si(111)-H-(1 × 1) [4]. The spectra also reveal umklapp mediated QWSs of similar intensity to those found in Ag/Ge(111) [7].

II. EXPERIMENTAL DETAILS

The measurements took place at the I4 beamline at the MAX-lab synchrotron radiation facility in Lund, Sweden. Base pressures were less than 1×10^{-10} Torr for the preparation chamber and less than 2×10^{-10} Torr for the analysis chamber. Pressure during Ga and Ag evaporation was below 4×10^{-10} Torr. The valence band measurements were obtained as two-dimensional images using a SPECS Phoibos 100 hemispherical electron analyzer with energy resolution of ≈50 meV and angular resolution of ±0.3°. Three photon energies were used: 21.2 eV and 40 eV for the valence band measurements and 130 eV for the core-level measurements. The angle between the incoming photons and the analyzer was 50°. Core-level spectra were recorded at normal emission, while the valence band spectra were recorded for a large range of emission angles, shifted in steps of 0.5° perpendicular to the analyzer angular direction. The Si(111) substrate was p type (boron doped) with a sheet resistance between 0.7 and 1.5 Ω cm. 0.43 ML of Ga was deposited onto a clean Si(111)-7 × 7 surface, followed by annealing at 600 °C for 2 min after which low-energy electron diffraction (LEED) showed a clear $(\sqrt{3} \times \sqrt{3})R30^\circ$ pattern [Fig. 1(a)]. Ag was evaporated from a Knudsen cell calibrated with a quartz crystal thickness monitor and deposited to the sample at RT. LEED measurements confirmed that the resulting Ag films were oriented in the (111) direction [see Fig. 1(b)]. All measurements took place at RT.

III. RESULTS AND DISCUSSION

A. LEED and core-level spectra

LEED patterns from the Ga/Si(111)-$\sqrt{3} \times \sqrt{3}$ surface as well as after deposition of a 3 ML and 9 ML Ag film are presented in Fig. 1. The LEED pattern of the 3 ML film [Fig. 1(b)] still exhibits faint $\sqrt{3} \times \sqrt{3}$ spots along with the bulk Si and Ag 1 × 1 spots. There are three possible origins for the $\sqrt{3}$ spots. According to the study by He *et al.* [31], the Ga/Si(111)-$\sqrt{3} \times \sqrt{3}$ surface was preserved underneath the Ag film, which could then be visible at very low thicknesses of Ag. Another cause could be the first layer after Ag deposition; the atomic rows of the island structure were separated by a distance equal to the distance between the Ga atoms on the Ga/Si(111)-$\sqrt{3} \times \sqrt{3}$ surface, as shown in the STM study by He *et al.* [31]. The third reason arises from a nonperfect film growth. If the Ag film does not smoothly cover the entire surface, but instead features empty patches or canyons where the bare Ga/Si(111) surface is exposed, this would result in the $\sqrt{3} \times \sqrt{3}$ pattern still being visible. Due to experimental restraints, no topography measurements were done on this sample. However, as canyons are common in Ag film growth on Si substrates [3], it is the most likely candidate for the presence of the $\sqrt{3} \times \sqrt{3}$ spots in the 3 ML LEED image. LEED pattern for the 9 ML silver film [Fig. 1(c)] exhibits predominantly contribution from the Ag film. The Ag 1 × 1 spots of the 3 ML LEED image have an elongated shape [see Fig. 1(b)]. This could occur if the surface has domains with small changes in the lattice angles. The Ag 1 × 1 spots in the LEED image of the 9 ML Ag film have a more circular shape compared to the 3 ML one, which indicates a higher degree of crystallinity within the film.

Figure 2 shows Ga 3d core-level photoelectron spectra taken both from the Ga/Si(111)-$\sqrt{3} \times \sqrt{3}$ surface and with a 3 ML Ag film. After removal of a Shirley type background, all the spectra were fitted using Voigt line shapes (a convolution of Lorentzian and Gaussian curves) with the program FITXPS [32]. The spectrum for the clean Ga/Si(111)-$\sqrt{3} \times \sqrt{3}$ surface can be fitted using two spin-orbit split components. Of these two, the main component is consistent with the T_4 adatom model of the Ga/Si(111)-$\sqrt{3} \times \sqrt{3}$ surface [33]. The second component most likely arises from interaction with defects on the surface, such as Si substitutional atoms. As the component is shifted to higher binding energy, the Ga atoms surrounding the defects must lose some of their charge. Each substitutional atom has, at the most, six Ga atoms surrounding it. The defects component has a relative intensity of 20%. Dividing this value by the number of Ga neighbors would thus provide an estimation of the number of defects on the surface. Assuming between three and six Ga neighbors per defect, depending on if they are isolated or grouped together, there are 3%–7% defects in the surface.

After deposition of 3 ML of silver, the Ga 3d spectrum undergoes a significant change. The spectrum has been

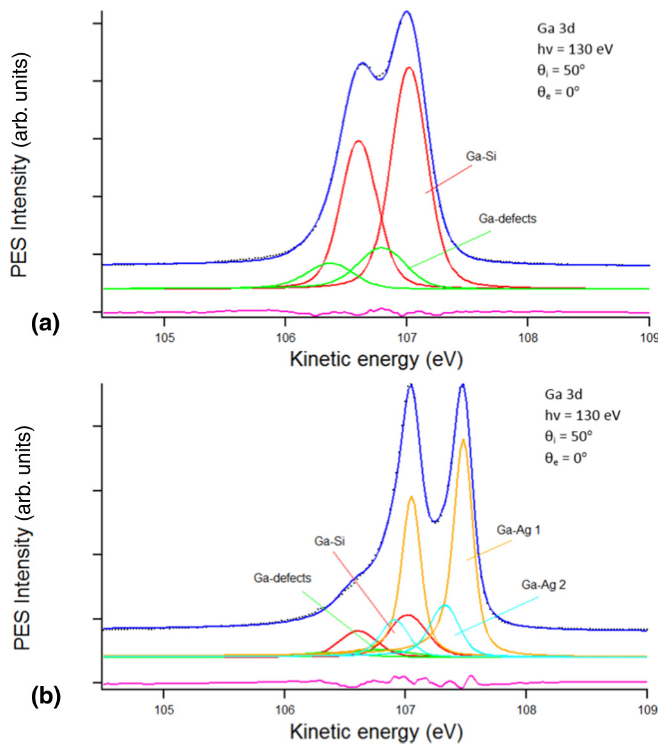

FIG. 2. Ga 3d core-level photoelectron spectra measured at normal emission with a photon energy of 130 eV. The spectrum in (a) is from the clean Ga/Si(111)-$\sqrt{3} \times \sqrt{3}$ surface, while (b) is with a 3 ML Ag film. The experimental data is represented by black dots, while the components, residue line, and total fit are all solid lines.

fitted using four components, two remaining from the Ga/Si interface, whereas the other two are asymmetric components (Doniach-Šunjić line shapes) shifted to lower binding energies by 0.31 eV and 0.46 eV, respectively. This type of asymmetric line shape is common for energy loss in metallic systems [34]. The sharp asymmetric shape of the raw peak and the energy shift of this new component both indicate that those Ga atoms must receive charge from the Ag atoms. The presence of two asymmetric components imply two different chemical shift configurations induced on Ga surrounded by the Ag atoms. As Ga has three bonds with Si, it could be possible for Ag to break either one or two of these, giving rise to two different chemical shifts. Consequently, these would result in line structures on the surface, as illustrated in Fig. 2 in Ref. [31]. The Ga-defects component has almost vanished in the 3 ML spectrum, as well as increased in Gaussian width. Most likely, this is because the small charge lost from the Ga atoms next to the defects is easily donated by the Ag atoms once the Ga-Ag bond is formed, and the small intensity component remaining in the spectrum comes from Ga atoms not yet covered by the Ag film. The intensity differences between the Ga-Si defects and the Ga-Ag components provide a means to estimate how much of the surface remains uncovered by the silver film. As the core-level electrons belonging to the two Ga-Ag components must travel through the Ag film, their relative intensity will be reduced in the measured spectrum. Assuming a mean free path (λ) of roughly 6 Å with a kinetic energy of 107 eV for the electrons traveling through the silver film and an exponential intensity decay with thickness (t) following $I = I_0 e^{-\frac{t}{\lambda}}$, the intensity of the two Ga-Ag components is reduced to approximately 30% of their initial values by the silver film. By comparison of the intensities from the Ga-Si and the Ga-defects components with the recalculated relative intensity of the two Ga-Ag components, the amount of empty patches in the film is found to be approximately 9%.

All fitting parameters are listed in Table I. The spin-orbit splitting used was 0.42 ± 0.005 eV for all components, which is in line with other results for Ga $3d_{5/2}$ [33,35]. Branching ratios were within 10% of the statistical value of 0.67. Further deposition of silver did not change the overall shape of the Ga 3d spectrum.

B. Valence band electronic structure

ARPES measurements of the valence band structure in the $\overline{\Gamma}$-$\overline{M}$ direction for silver films with thicknesses ranging from 3 to 12 ML are shown in Fig. 3. Binding energies are defined with respect to the Fermi level ($E_F = 0$ eV). The strong photoemission intensity around $k_\parallel = 0$ Å^{-1} at the Fermi level is identified as the Shockley surface state (marked SS) of Ag(111) [2,13,16], which is visible for all measurements. The SS becomes more sharp and intensive with increased Ag film thicknesses. This feature of the SS has previously been used to determine the crystallinity of the Ag film [4,13]. The SS band sharpness observed for films of 6 ML thickness and above suggests highly crystalline and nonstrained Ag films. The diffuse SS observed for the 3 ML Ag film is caused by coupling with the substrate. As the SS moves to higher binding energies with decreased film thicknesses, the bottom of the state band is brought close to the bulk Si valence band edge, which allows for the two to couple with each other. This will reduce the SS band sharpness. The presence of clearly visible and well defined quantum-well states for the 3 ML film indicates that, even if the film morphology features many canyons, the majority of the film is dominated by one thickness.

Well defined QWSs with parabolic in-plane dispersions can be observed already for a 3 ML thick film. As the film thickness increases, the QWSs move towards lower binding energies and more states appear. For the 3 ML spectrum, the bulk Si sp valence band appears to be visible. In the energy region outside of this band, the QWSs are fully confined in the thin silver film, resulting in strong photoemission features. As the QWSs intersect with the projected bulk Si valence bands, which can be seen around -0.9 eV and $k_\parallel \approx 0.2$–0.4 Å^{-1} for the 3 ML spectrum, the states start to couple with the electronic structure of the substrate and abruptly bend up to follow the Si bulk bands. At the same time, a resonant type of QWS is formed inside the Si valence band region, with a resulting drop in the photoemission intensity. For Ag film thicknesses higher than 3 ML, the projected Si bulk bands gradually decrease in visibility. However, the effect of the substrate can still be seen in the behavior of the QWSs. As they move from being fully confined to resonant states, the intensity drops and a change in their parabolic dispersions is clearly visible as kinks. This corresponds to a change in effective mass, which is higher for the fully confined part of the QWSs compared to the resonant part. Since the film/substrate

TABLE I. Fitting parameters for the Ga 3d core-level spectra in Fig. 2. Both the clean Ga/Si(111)-$\sqrt{3} \times \sqrt{3}$ and the 3 ML Ag film spectra are included.

	Ga/Si(111)		3 ML Ag film			
Parameter/component	Ga-Si	Ga defects	Ga-Si	Ga defects	Ga-Ag 1	Ga-Ag 2
Main peak E_k (eV)	107.02	106.81	107.02	106.81	107.48	107.33
Spin-orbit split (eV)	0.42	0.42	0.42	0.42	0.42	0.42
Branching ratio	0.67	0.63	0.62	0.62	0.74	0.72
Gaussian FWHM	0.30	0.40	0.32	0.52	0.13	0.22
Lorentzian FWHM	0.10	0.10	0.10	0.10	0.10	0.10
Asymmetry value	0.00	0.05	0.00	0.05	0.05	0.05
Intensity (%)	80.02	19.98	18.61	5.40	56.67	19.33

electronic coupling effects are stronger for the thinner films, the QWSs photoemission features become broader.

The ARPES spectra also show a second type of quantum-well state, which can be seen in Fig. 4. They are the result of umklapp scattering and have previously been studied in detail for the Ag/Ge(111) system by Tang *et al.* [7]. A constant energy surface of the surface Brillouin zone (SBZ) [Fig. 4(a)], obtained by stitching together spectra from different emission angles with a computer program, shows the umklapp-mediated QWSs shaped as ovals centered around the $\overline{M}$ points of the Si (1×1) SBZ. The figure also shows the regular type of QWSs which are centered around the $\overline{\Gamma}$ point. The first QWS marked $n = 1$ has a roughly hexagonal-like shape. This hexagonal shape is still visible for the $n = 2$ state even though it has become more rounded. Looking at $n = 3$, the curved form is more prominent and the state is no longer hexagonal in nature. This hexagonal shape of some QWSs was explored for Ag/Ge(111) by Moras *et al.* [36] and is the result of hybridization between the QWSs and the bulk Si valence bands. This coupling occurs when a QWS is in proximity to the valence band, and as such different QWSs will take on a hexagonal shape at different binding energies. Moras *et al.* compared the behavior of the hexagonal shape of the QWSs with those of a freestanding slab of Ag. It was found that, without taking the substrate into account, the QWSs become more hexagonal the closer they move to the edge of the SBZ. Since the hexagonal shape of the QWSs in Fig. 4(a) is more pronounced towards the center of the SBZ, this shape must be caused by coupling with the substrate. Exploring the shape of the QWSs with binding energies shows they can take on a hexagonal shape of two different orientations, similar to the case for Ag/Ge(111). This is due to the difference in symmetry between the bulk Si light and heavy hole valence bands. The ripples visible in quantum-well states 4 and 5, to the left of the line around $k_{x\parallel} \approx -0.7$ Å^{-1} in Fig. 4(a), are caused by the umklapp states.

The umklapp-mediated QWSs are visible in Fig. 4(b) between the Fermi level and -1.3 eV binding energy, centered around $k_{y\parallel} \approx \pm 0.45$ Å^{-1} [the two $\overline{M}$ points of the Si(111) SBZ]. As can be seen in Fig. 4(b), the umklapp-mediated quantum-well states have a smaller binding energy interval between them compared to the normal type of QWSs from the same film thickness [see Fig. 3(c)]. The energy spacing of the umklapp states for a 9 ML Ag film is about 0.3–0.4 eV, compared to approximately 0.9–1.1 eV for the regular QWSs. The umklapp-mediated states show up in ARPES spectra for all the measured film thicknesses, with energy spacing of 1/3–1/2 compared with that of the regular quantum-well states for the

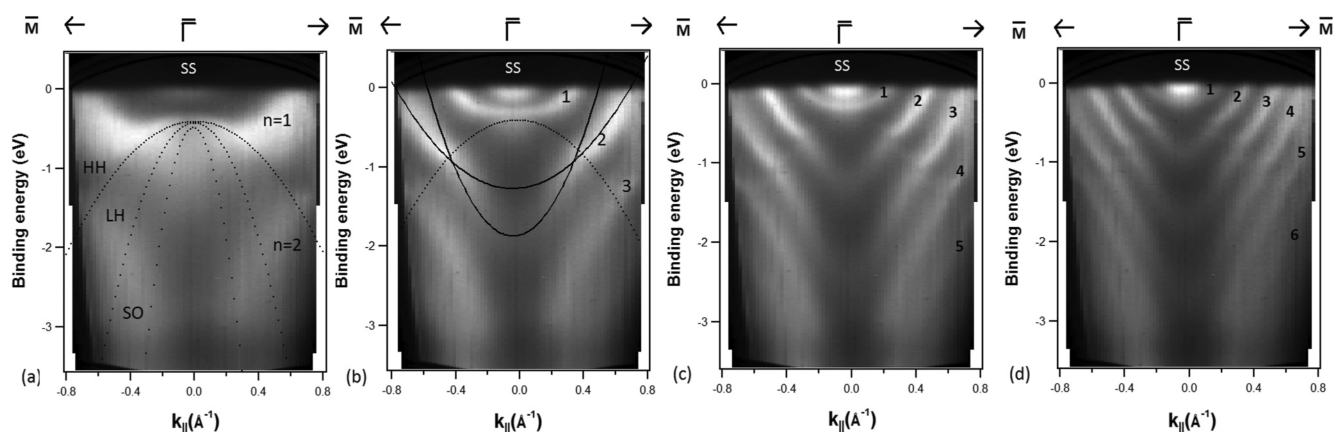

FIG. 3. Valence band structure measurements (ARPES data) of Ag film on a Ga/Si(111)-$\sqrt{3} \times \sqrt{3}$ surface in the $\overline{\Gamma}$-$\overline{M}$ direction of the SBZ with thickness of (a) 3 ML, (b) 6 ML, (c) 9 ML, and (d) 12 ML. Photon energy was 40 eV for all measurements. The Shockley surface state is marked with SS and the quantum-well states numbered starting from $n = 1$. The dotted lines in (a) and (b) show the edges of the bulk Si valence bands, whereas the filled parabolic lines in (b) are fitted to the $n = 2$ quantum-well state, one to the region above the Si valence band and the other below.

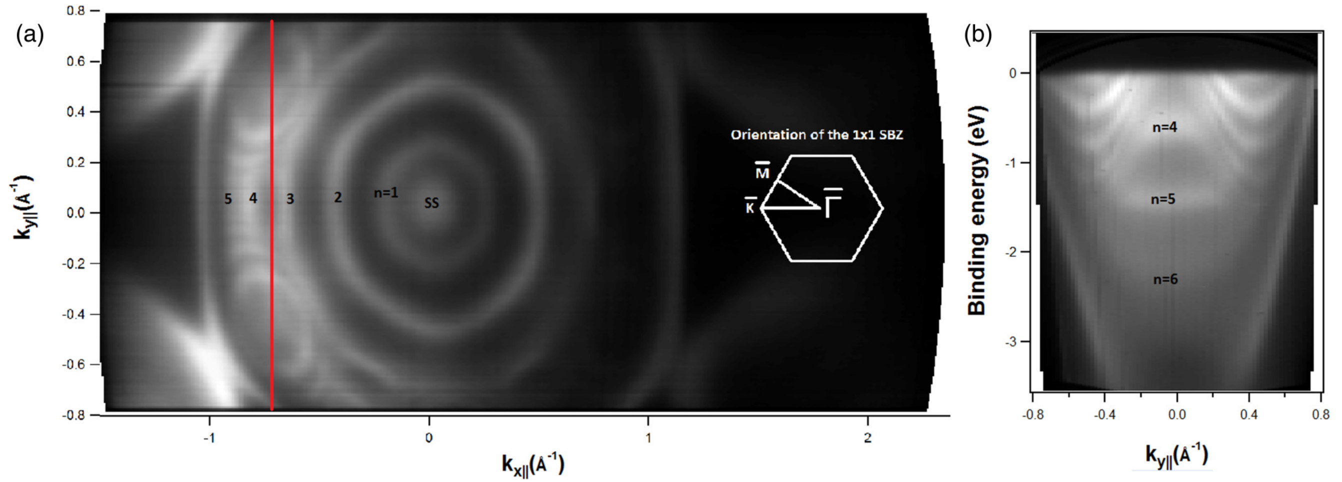

FIG. 4. (a) Constant energy surface (≈ -0.15 eV below E_F) for a 9 ML Ag film ($h\nu = 40$ eV). The $k_{x\parallel}$ vector runs parallel to the $\overline{\Gamma}$-$\overline{K}$ direction of the (1×1) SBZ, whereas the $k_{y\parallel}$ vector is parallel to the $\overline{\Gamma}$-$\overline{M}$ direction (the $\overline{\Gamma}$ point is located at $k_{y\parallel} = k_{x\parallel} = 0$). The Shockley surface state is marked with SS and the quantum-well states numbered starting from $n = 1$. The line between the $n = 3$ and $n = 4$ subbands shows the approximate placement of the spectrum in (b). (b) Valence band measurements from a 9 ML Ag film on the Ga/Si(111)-$\sqrt{3} \times \sqrt{3}$ surface taken with photon energy of 40 eV. The spectrum is recorded between two $\overline{M}$ points of the Si(111) 1×1 SBZ, with a $k_{x\parallel}$ value of ≈ -0.7 Å^{-1}, as indicated by the line in the constant energy surface shown in (a).

same thickness. This is comparable with the result observed by Tang *et al.* [7], where they reported a ratio of roughly 1/2 for a 13 ML Ag film.

In previous studies of Ag films on Si(111) substrates, well-defined quantum-well state features are only observed starting from a 5–6 ML film thickness [2–4]. The existence of QWSs for even lower coverages on the Ga/Si(111)-$\sqrt{3} \times \sqrt{3}$ surface enables the possibility to more closely study film/substrate interactions and interface effects. In order to compare the results with other works, the QWSs have been analyzed within the framework of the phase accumulation model.

Quantum-well state formation in thin films occurs from spatial confinement of the electrons in the direction perpendicular to the substrate surface. The spatial confinement leads to a quantization of the bulk Ag *sp* valence states in the (111) direction. This results in a $k_\perp$-vector dependence with the film thickness for the QWSs, which is described through the Bohr-Sommerfeld quantization condition [17]:

$$2k_\perp d + \phi_{\text{tot}} = 2\pi n, \tag{1}$$

where $k_\perp$ is the electron wave vector normal to the surface, d the film thickness, n the principal quantum number for the QWS, and ϕ_{tot} the total phase shift of the electron wave on reflection at the two boundaries, which are assumed to be additive ($\phi_{\text{sub}} + \phi_{\text{vac}}$). This case is similar to that of a "particle in a box," where the electron forms a standing wave restricted by the box dimension, with the addition of the boundary phase shift. The phase shift is introduced due to the nonperfect reflection of the electron wave at the two boundaries: film/substrate and film/vacuum. This shift depends on the binding energy of the QWS, and is approximated as a linear function of energies. Calculating the value of $k_\perp$ can be done through the simultaneous solution of Eq. (1) for two QWSs with the same binding energy (E_B) but with different values of the quantum number n, and from two different film thicknesses. This results in the following equation:

$$k_\perp = \pi \frac{n' - n}{d' - d}. \tag{2}$$

Since the quantum-well states are formed from a quantization of the Ag *sp* bulk valence state band in the (111) direction, the QWSs binding energies can be used to reproduce the bulk band structure in this direction [13]. Fitting the experimental data of E_B and $k_\perp$ obtained from Eq. (2) to the bulk band can thus be used to estimate the film thickness. The Ag bulk band is described with the two-band nearly free electron model:

$$E(k_\perp) = E_0 - [ak_\perp^2 + U - (4a^2bk_\perp^2 + U^2)^{1/2}], \tag{3}$$

with $a = \hbar^2/2m_\perp^*$ and $b = 3\pi^2/a_0^2$. E_0 is the relative position of the Ag *sp* band edge compared to the E_F and U half the *sp* band gap at the L point of the Ag Brillouin zone. The values used in the calculations presented here are $E_0 = 0.31$ eV and $U = 2.1$ eV [16], with $a_0 = 4.09$ Å (the lattice constant of bulk Ag) [4]. The value of $m_\perp^*$ [effective mass of the band in the (111) direction] is typically found to be between $0.7m_0$ and $0.8m_0$ [3,4,13,16]. A plot of a least mean square (LMS) fit of Eq. (3) to the experimental data is shown in Fig. 5. Due to a limited data range, only three experimental points were obtained. The fit gives the value of $m_\perp^* = 0.79m_0$. This is almost the same as that obtained by Matsuda *et al.* [3] for Ag/Si(001), close to that of Ag/Cu(111) [13], as well as the one used for Ag/graphite(0001) [16] and Ag/Si(111)-H-(1×1) [4]. These bulk band calculations are plotted in Fig. 5 along with the experimental data for Ga/Si(111)-$\sqrt{3} \times \sqrt{3}$. The accuracy of the QWSs' energy positions is estimated to ≈ 0.2 eV.

The total phase shift of the two boundaries, $\phi_{\text{tot}}(E)$, is calculated through the *structure plot*, which tracks the evolution of the quantum-well states binding energies with film thicknesses. A structure plot is obtained by solving Eq. (1) for thickness (d) and Eq. (3) for $k_\perp(E)$. Binding energies were extracted by a simulation method illustrated in Fig. 3(b) from

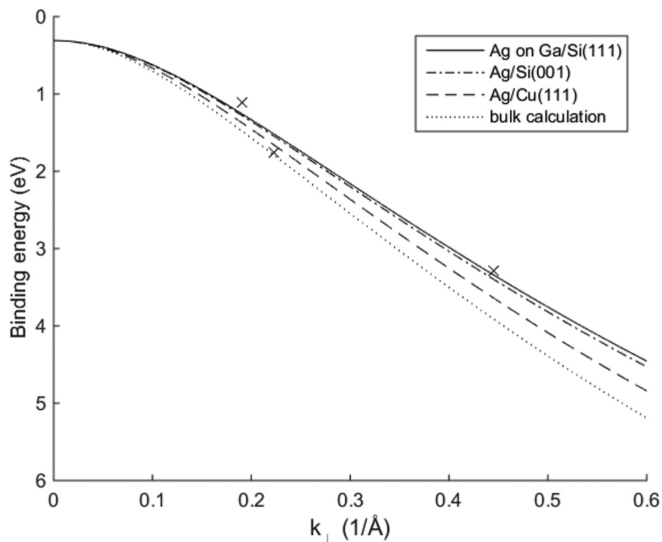

FIG. 5. Bulk Ag energy dispersion for the *sp* band along the $\overline{\Gamma}$ to $\overline{L}$ line of the BZ. Black crosses represent experimental data points from Ag films on the Ga/Si(111)-$\sqrt{3} \times \sqrt{3}$ surface. The lines are calculations based on the two-band nearly free electron model. Filled line is based on $0.79m_0$, a LMS fit to the experimental data, dash-dot line is $0.78m_0$ from Ag/Si(001) [3], dashed line $0.74m_0$ from Ag/Cu(111) [13], and dotted $0.70m_0$ from bulk calculations [4,16].

the experimental data at the bottom of the resonant QWSs. The fit for the resonant states (lower part) was chosen in order to make the structure plot consistent with other works [3,4]. For increased accuracy, data from photoemission spectra using both 40 eV and 21.2 eV photon energy were included. The experimentally observed binding energies are plotted along with the theoretical calculation in Fig. 6. Best fit for the total phase shift was found to be $\phi_{\text{tot}}(E) = -0.29(eV^{-1})\pi \times E + 0.82\pi$ (see Fig. 7). The first quantum-well state, $n = 1$,

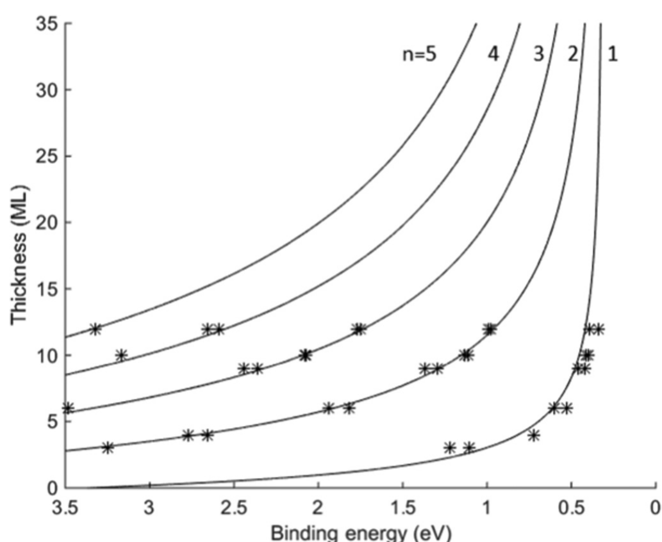

FIG. 6. Structure plot showing the QWSs binding energy positions with respect to film thicknesses for Ag film on Ga/Si(111)-$\sqrt{3} \times \sqrt{3}$. Black lines represent model calculations, whereas black asterisks are experimentally obtained energy positions.

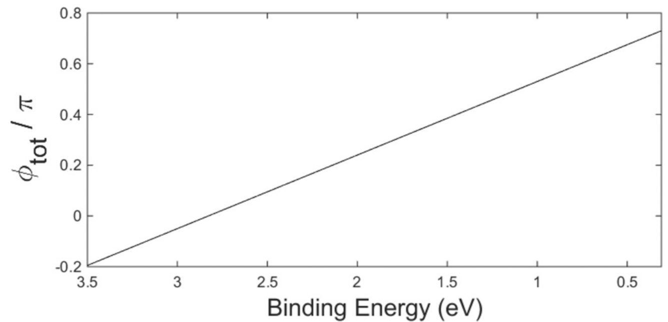

FIG. 7. Total phase shift ϕ_{tot} as a function of quantum-well state binding energies for Ag films on the Ga/Si(111)-$\sqrt{3} \times \sqrt{3}$ surface obtained from fitting to the *structure plot*.

has the largest error between the calculated binding energies and experimental points for all thicknesses. This is most likely due to a combination of two effects. First, as the film thickness becomes very small, in the 3–4 ML range, substrate and interface effects on the QWSs are expected to become more dominant, which may invoke changes to the phase shift. Secondly, as the QWSs binding energies decrease and they move out of the bulk Si valence band energy region, around −0.5 eV binding energy, the phase shift may also change. For the majority of the QWSs, however, the simple approximation of a phase shift with linear energy dependence holds very well. A comprehensive comparison of phase shifts for Ag films on different Si substrates has been made by Arranz *et al.* [4]. As can be seen in Fig. 7, the phase shift for Ag films on the Ga/Si(111)-$\sqrt{3} \times \sqrt{3}$ surface has a negative slope with the binding energy and has a mostly positive value in the measured energy window. The phase shift thus shows a behavior which is common for metal-on-semiconductor systems.

The total phase shift can further be split up into two parts: ϕ_{vac} at the film/vacuum boundary and ϕ_{sub} at the film/substrate interface. It has previously been established that ϕ_{vac} can be explained as an image potential in the WKB approximation [37]:

$$\phi_{\text{vac}} = \pi \sqrt{\frac{3.4(eV)}{(E_v - E)}} - \pi, \tag{4}$$

where E_v is the vacuum level, which has a value of 4.5 eV for Ag(111). Evaluating this at the Fermi level, one obtains a value of $\phi_{\text{vac}}(E_F) = -0.13\pi$. The total phase shift at the Fermi level for Ag films was found to be 0.82π based on the simple linear expectation of the phase shift. This gives $\phi_{\text{sub}} = \phi_{\text{tot}} - \phi_{\text{vac}} = 0.95\pi$. As the substrate is semiconducting, reflection in the band gap region should be the ideal Bragg case (π). The calculated phase shift is very close to this value, which indicates good reflection properties of the Ga/Si(111)-$\sqrt{3} \times \sqrt{3}$ interface.

One important characteristic which determines the properties of the quantum-well states is the in-plane effective mass ($m_{\parallel}^*$). As can be seen in Fig. 3, the QWSs follow a parabolic dispersion relation so that

$$E(k_{\parallel}) = E_0 + \frac{\hbar^2 k_{\parallel}^2}{2m_{\parallel}^{*2}}, \tag{5}$$

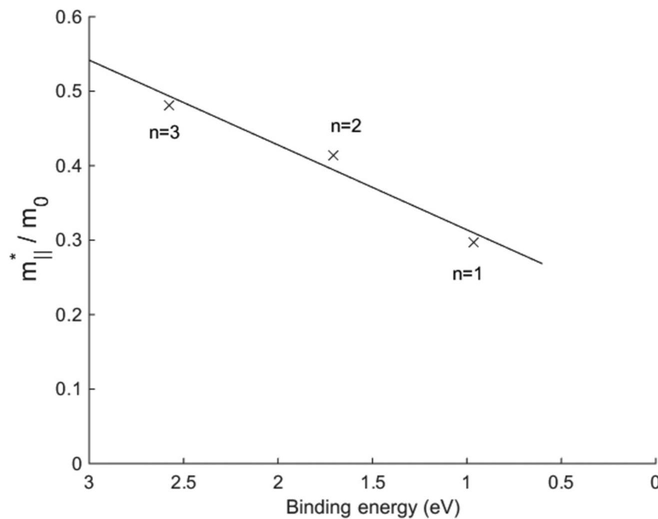

FIG. 8. In-plane effective mass as function of binding energies for the resonant QWS region taken from a 12 ML Ag film on Ga/Si(111)-$\sqrt{3} \times \sqrt{3}$. Black crosses represent calculated masses from experimental data. The quantum number, n, of each quantum-well state is indicated next to the data point. The black line is a guide for the eye.

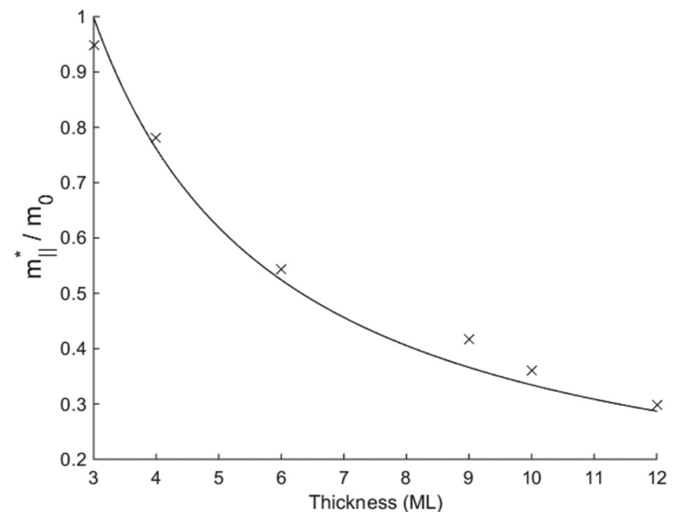

FIG. 9. Tracking the in-plane effective mass of the resonant region of the second quantum-well state ($n = 2$) with respect to Ag film thicknesses. Black crosses are experimental values, whereas the black line is proportional to a $1/N$ function.

where E_0 is the energy at $k_\perp = 0$ and $m^*_\parallel$ is the effective mass of the electrons in the band. The figure shows that the QWSs undergo a clear change in effective mass as they leave the region of the bulk Si valence band and move from being resonant states to fully confined ones. One can therefore investigate the effective mass properties of the two regions separately. In order to compare with other studies, $m^*_\parallel$ has been calculated for the resonant part of the QWSs, around the state subband center at $k_\parallel = 0$. To investigate how the effective mass changes with the binding energy, QWSs from a 12 ML thick Ag film were used (see Fig. 8). This spectrum was chosen as it has the most resonant QWSs in the measured energy window of the film thicknesses studied. Figure 8 shows that $m^*_\parallel$ lies in the range between $0.29m_0$ and $0.50m_0$, and that they follow an increasing trend with binding energies. While the same range of values was reported by Matsuda *et al.* [3] for Ag films on Si(111) and Si(001), they instead found a decreasing trend of $m^*_\parallel$ with the QWSs binding energies. This highlights the importance of the interface for the behavior of the quantum-well states. The difference between Si(111) and Ga/Si(111)-$\sqrt{3} \times \sqrt{3}$ lies in the dangling bonds. On the Ga/Si(111)-$\sqrt{3} \times \sqrt{3}$ surface, the Ga atoms have terminated all the Si dangling bonds. A similar increasing trend of $m^*_\parallel$ with QWSs binding energies has been reported for Ag films on other passivated surfaces [4,9,12,13]. Theoretical band structure calculations of bulk Ag [13] also generate an in-plane effective mass behavior which increases with the binding energy, with values in the $0.2m_0$–$0.5m_0$ range. This behavior is attributed to hybridization between the Ag *sp* states and the 4*d* states as explained by Matsuda *et al.* [3]. As the Ag films on the Ga/Si(111)-$\sqrt{3} \times \sqrt{3}$ system show a similar trend, it confirms that the Ga/Si(111)-$\sqrt{3} \times \sqrt{3}$ substrate can be used to grow Ag films with high quality at room temperature.

The change in effective mass of the resonant part of the QWSs with respect to thickness is plotted in Fig. 9. It tracks how $m^*_\parallel$ of the second quantum-well state ($n = 2$) changes with film thicknesses between 3 and 12 ML. As can be seen, the effective mass increases with decreasing film thicknesses. This is an effect that was investigated in detail for Ag/Ge(111) by Tang *et al.* [9], and is related to the phase shift, whose effect on $m^*_\parallel$ decreases as a $1/N$ function. In short, the thinner the film, the more prominent the effect of the film boundaries will be. Simply following one QWS may be a very crude representation, as one could make an argument that the states will also move in binding energies, which according to Fig. 8 would also give an increase of the effective mass. However, as the highest $m^*_\parallel$ obtained for the 12 ML thick Ag film was lower than $0.50m_0$, and $m^*_\parallel$ for the 3 ML film goes up to almost $0.95m_0$, the binding energy shift alone cannot explain this increase.

Figure 10 shows the effective mass change for the fully confined part of the QWSs with respect to binding energies for a number of thicknesses from 3 to 12 ML. These $m^*_\parallel$ values are significantly higher compared to those of the resonant parts, ranging from $0.90m_0$ to $2.70m_0$. A sharp increase of $m^*_\parallel$ with reduced film thicknesses is clearly visible in the plot. The fully confined part of the QWSs still exhibits the same trend of increasing effective mass with the binding energies. While the $m^*_\parallel$ trend still follows the behavior of theoretical Ag bulk calculations, the values are much higher in this region, especially for low thickness films. Since this part of the QWSs exists in the Si band gap region, it is unlikely that the increase occurs because of hybridization with the substrate. One explanation could be phase shift effects. The substrate phase shift, ϕ_{sub}, is different for the fully confined QWSs in the Si band gap region compared to the resonant QWSs inside the bulk Si valence band region [3]. This phase shift was previously shown to play a role in the in-plane effective mass of QWSs, particularly in the low ML regime [9]. The phase shift discontinuity has been previously suggested by Matsuda *et al.* in order to explain an observed band splitting of some of the QWSs [3], which also comes with a change

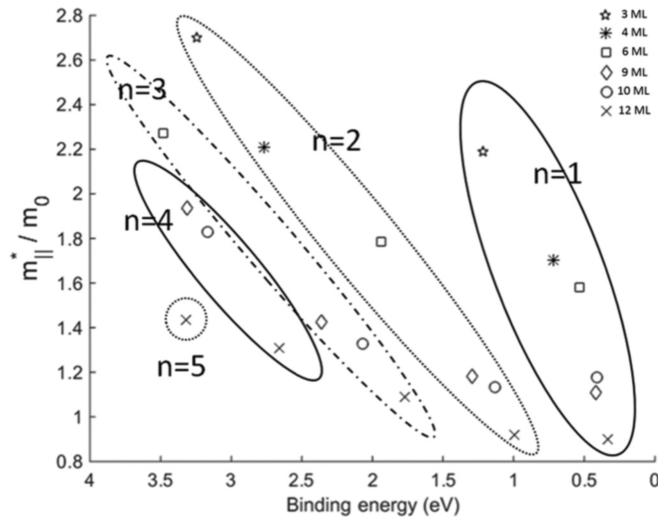

FIG. 10. In-plane effective mass of the fully confined part of the QWSs with respect to binding energies. Experimental values from the same thickness have the same symbol. Data belonging to QWSs of the same quantum number are encircled together. The ARPES spectra used to calculated the effective masses were taken with a photon energy of 40 eV.

in effective mass of the electrons in the band. The splitting is caused by the coupling of the QWSs with the substrate bulk bands. This coupling interaction originates from the interface. In a simple picture, it may affect the phase shift and in turn the effective mass.

Due to their oval shape, the in-plane effective mass of the umklapp quantum-well states is anisotropic in nature. Calculations of the effective mass across the Si(111) 1×1 $\overline{M}$ point in the direction parallel to $k_{y||}$ in Fig. 4(a) give values between $0.3m_0$ and $0.5m_0$. The effective mass is slightly lower when measured across the $\overline{M}$ point in the direction parallel to $k_{x||}$. For both of these effective mass values, there appears to be no major change with thicknesses, and the trend is shifted towards lower $m^*_{\parallel}$ with increased binding energies. This is in contrast to the cases for the normal QWSs. One explanation could be the grazing angle of the electron wave for umklapp-reflected states. This would result in less interaction with the substrate. The effect of the substrate phase shift would thus be lower for the umklapp states, resulting in low effective mass even for the thinner films. The $m^*_{\parallel}$ relationship between the two types of states deserves further study.

IV. SUMMARY AND CONCLUSIONS

Ag thin films have been created on the Ga/Si(111)-$\sqrt{3} \times \sqrt{3}$ surface by deposition in room temperature conditions. Both valence bands and core levels have been studied by photoemission. The measurements show that the band structure contains the standard QWSs and umklapp mediated quantum-well states at the $\overline{M}$ points of the Si(111) 1×1 SBZ. QWSs have been observed in a 3 ML film, an indication that the Ag thin films are of high quality even for a very low coverage. This allows for a more in-depth study of coupling effects between the electronic structures of the film and the substrate. In addition, the characteristics of the QWSs have been studied thoroughly. The phase accumulation model has been successfully explored to analyze the QWSs binding energies dependence on film thicknesses, as well as the total phase shift of the electron wave with boundary reflection. In-plane effective mass behavior of the QWSs has been examined and compared with similar thin film systems. The behavior is found to be consistent with Ag films on those passivated surfaces. These results open a new opportunity for studying interface and substrate interaction effects, which modify the characteristics of quantum-well states in thin films.

ACKNOWLEDGMENTS

This work was supported by the Swedish Research Council (Contract No. 2013-5291). The MAX-lab staff are acknowledged for their help during the experiment.

[1] T. C. Chiang, Surf. Sci. Rep. **39**, 181 (2000).
[2] A. L. Wachs, A. P. Shapiro, T. C. Hsieh, and T. C. Chiang, Phys. Rev. B **33**, 1460 (1986).
[3] I. Matsuda and H. W. Yeom, J. Electron Spectrosc. Relat. Phenom. **126**, 101 (2002).
[4] A. Arranz, J. F. Sanchez-Royo, J. Avila, V. Perez-Dieste, P. Dumas, and M. C. Asensio, Phys. Rev. B **65**, 195410 (2002).
[5] S. J. Tang, T. Miller, and T. C. Chiang, Phys. Rev. Lett. **96**, 036802 (2006).
[6] N. J. Speer, S.-J. Tang, T. Miller, and T.-C. Chiang, Science **314**, 804 (2006).
[7] S. J. Tang, Y. R. Lee, S. L. Chang, T. Miller, and T. C. Chiang, Phys. Rev. Lett. **96**, 216803 (2006).
[8] Y. Liu, N. J. Speer, S. J. Tang, T. Miller, and T. C. Chiang, Phys. Rev. B **78**, 035443 (2008).
[9] S. J. Tang, W. K. Chang, Y. M. Chiu, H. Y. Chen, C. M. Cheng, K. D. Tsuei, T. Miller, and T. C. Chiang, Phys. Rev. B **78**, 245407 (2008).
[10] M. K. Brinkley, N. J. Speer, Y. Liu, T. Miller, and T.-C. Chiang, Europhys. Lett. **96**, 67013 (2011).
[11] H. M. Zhang, L. J. Holleboom, and L. S. O. Johansson, Phys. Rev. B **96**, 041402 (2017).
[12] S. K. Mahatha and K. S. R. Menon, J. Phys.: Condens. Matter **25**, 115501 (2013).
[13] M. A. Mueller, T. Miller, and T. C. Chiang, Phys. Rev. B **41**, 5214 (1990).
[14] N. B. Brookes, Y. Chang, and P. D. Johnson, Phys. Rev. Lett. **67**, 354 (1991).
[15] J. E. Ortega, F. J. Himpsel, G. J. Mankey, and R. F. Willis, Phys. Rev. B **47**, 1540 (1993).
[16] F. Patthey and W.-D. Schneider, Phys. Rev. B **50**, 17560 (1994).
[17] N. V. Smith, N. B. Brookes, Y. Chang, and P. D. Johnson, Phys. Rev. B **49**, 332 (1994).
[18] T. Valla, P. Pervan, M. Milun, A. B. Hayden, and D. P. Woodruff, Phys. Rev. B **54**, 11786 (1996).

[19] R. K. Kawakami, E. Rotenberg, E. J. Escorcia-Aparicio, H. J. Choi, T. R. Cummins, J. G. Tobin, N. V. Smith, and Z. Q. Qiu, Phys. Rev. Lett. **80**, 1754 (1998).
[20] J. J. Paggel, T. Miller, D. A. Luh, and T. C. Chiang, Appl. Surf. Sci. **162-163**, 78 (2000).
[21] L. Aballe, C. Rogero, P. Kratzer, S. Gokhale, and K. Horn, Phys. Rev. Lett. **87**, 156801 (2001).
[22] L. Aballe, C. Rogero, S. Gokhale, S. Kulkarni, and K. Horn, Surf. Sci. **482-485**, 488 (2001).
[23] L. Aballe, C. Rogero, and K. Horn, Phys. Rev. B **65**, 125319 (2002).
[24] D. A. Ricci, T. Miller, and T.-C. Chiang, Phys. Rev. Lett. **93**, 136801 (2004).
[25] C. Koitzsch, C. Battaglia, F. Clerc, L. Despont, M. G. Garnier, and P. Aebi, Phys. Rev. Lett. **95**, 126401 (2005).
[26] F. Schiller, R. Keyling, E. V. Chulkov, and J. E. Ortega, Phys. Rev. Lett. **95**, 126402 (2005).
[27] A. M. Shikin and O. Rader, Phys. Rev. B **76**, 073407 (2007).
[28] T. Hirahara, T. Nagao, I. Matsuda, G. Bihlmayer, E. V. Chulkov, Y. M. Koroteev, and S. Hasegawa, Phys. Rev. B **75**, 035422 (2007).
[29] A. M. Shikin, A. G. Rybkin, D. E. Marchenko, D. Y. Usachov, V. K. Adamchuk, A. Yu. Varykhalov, and O. Rader, Phys. Solid State **52**, 1515 (2010).
[30] M.-K. Lin, Y. Nakayama, C.-H. Chen, C.-Y. Wang, H.-T. Jeng, T.-W. Pi, H. Ishii, and S.-J. Tang, Nat. Commun. **4**, 2925 (2013).
[31] J.-H. He, L.-Q. Jiang, J.-L. Qiu, L. Chen, and K.-H. Wu, Chin. Phys. Lett. **31**, 128102 (2014).
[32] D. N. Adams and J. L. Andersen, FITXPS v. 2.12.
[33] K. Higashiyama, S. Kono, T. Kinoshita, T. Miyahara, H. Kato, H. Ohsawa, Y. Enta, F. Maeda, and Y. Yaegashi, Surf. Sci. Lett. **186**, 568 (1987).
[34] A. Flodström, R. Nyholm, and B. Johansson, in *Synchrotron Radiation Research*, edited by R. Z. Bachrach (Plenum Press, New York, 1992), p. 199.
[35] J. Čechal, M. Kolíbal, P. Kostelník, and T. Šikola, J. Phys.: Condens. Matter **19**, 016011 (2007).
[36] P. Moras, D. Topwal, P. M. Sheverdyaeva, L. Ferrari, J. Fujii, G. Bihlmayer, S. Blügel, and C. Carbone, Phys. Rev. B **80**, 205418 (2009).
[37] E. McRae and M. Kane, Surf. Sci. **108**, 435 (1981).